A Fully Flexible Temperature Sensor for Wearable Applications

Maxx A. Seminario, Ayden Uerling, Sina Balkır, Michael W. Hoffman
University of Nebraska-Lincoln,
Department of Electrical Engineering,
Lincoln, NE 68588-0511, USA
{mseminario2@huskers.unl.edu, auerling3@huskers.unl.edu, sbalkir@unl.edu, mhoffman1@unl.edu}

Joseph A. Schmitz
University of Nebraska-Lincoln,
School of Computing,
Lincoln, NE 68588-0150, USA
{jschmitz67@unl.edu}

Eric J. Markvicka
University of Nebraska-Lincoln,
Department of Mechanical and Materials Engineering,
Lincoln, NE 68588-0526, USA
{eric.markvicka@unl.edu}

2025 IEEE International Symposium on Circuits and Systems (ISCAS) | 979-8-3503-5683-0/25/$31.00 ©2025 IEEE | DOI: 10.1109/ISCAS56072.2025.11043365

***Abstract*— This paper presents the design of a fully flexible temperature sensor for wearable applications. The sensor is implemented using the newly available flexible integrated electronic circuit (Flex-IC) technology from Pragmatic Semiconductor [1]. To address the design challenges due to the limited set of thin film components available in this non-CMOS technology, a counter-based time-to-digital conversion (TDC) technique has been developed, where the pulses provided by a temperature-dependent ring oscillator are gated and counted by a temperature-independent delay cell. The operation of the delay cell relies on the temperature coefficient cancellation of resistive components by a cross-coupled pair. A tunable calibration mechanism is also incorporated in the design to handle the process corners in a temperature range of $32\,^{\circ}\mathrm{C}$ - $42\,^{\circ}\mathrm{C}$ suitable for biological sensing. The presented sensor design exhibits a low time-jitter induced measurement error, with a $0.81\,\%$ probability of toggling the least significant bit (LSB) per sample, maintaining $0.1\,^{\circ}\mathrm{C}$ precision and a zero-error range of $6.8\,^{\circ}\mathrm{C}$, while dissipating a power of $2.5\,\mathrm{mW}$ with an acquisition time of $3\,\mathrm{ms}$. The chip layout measures $3.0\,\mathrm{mm}\times 3.0\,\mathrm{mm}$ with a die thickness of $30\,\mu\mathrm{m}$. Compared to existing rigid and hybrid systems, the Flex-IC technology opens up opportunities for advancing conformal electronics, particularly for applications requiring continuous monitoring on dynamic body surfaces.**

I. Introduction

The form factors of bioelectronics are constantly evolving to create devices that are thinner, lighter, and more compact, with the common goal of providing intimate contact with biological tissue to improve signal quality. While significant advances have been made, ultrathin systems often face limitations in functionality and robustness, presenting challenges in manufacturing, handling, and real-world deployment [2], [3], [4]. Flexible hybrid electronic systems are promising, offering a balance between flexibility and electronic capabilities [5], [6]. However, current flexible hybrid systems often fail to achieve the thinness and conformability necessary for intimate integration with biological systems. This paper explores a novel approach to address these challenges for temperature monitoring by focusing on the combination of innovative materials and Flex-IC technologies that could broadly impact the fields of wearable electronics, soft robotics, and building integrated electronics.

Biological temperature monitoring is essential in various applications, including medical diagnostics, wearable devices, and animal health monitoring. There is significant demand for temperature sensing solutions that target flexible and mechanically compliant applications. Existing approaches employ a hybrid combination of flexible/stretchable substrates and rigid temperature-sensing electronic circuit components that limit their ability to conform to three-dimensional shapes [6], [7], [8]. These systems rely on commercial off-the-shelf (COTS) components, such as silicon-based sensors and rigid discrete components, which can be inflexible and uncomfortable for long-term use on dynamic body surfaces. These limitations hinder their effectiveness in applications requiring conformal contact due to low thermal coupling. Recent work also explores creating temperature sensor components based on novel materials, fabrics, and printed electronics. However, this category of sensors are passive in nature and require additional peripheral electronics for full functionality [9], [10], [11].

This paper presents a completely flexible, mechanically compliant, and highly integrated temperature sensor design by implementing a custom temperature sensor with digital readout in a Flex-IC design that can be integrated with an elastomeric substrate. The sensor is realized through the newly available Flex-IC technology from Pragmatic Semiconductor [1], featuring a minimum bend radius of $5\,\mathrm{mm}$, a minimum transistor channel length of $600\,\mathrm{nm}$, and a die thickness of $30\,\mu\mathrm{m}$. Hence, the sensor avoids the constraints of traditional integrated electronic circuits and systems, providing a high level of mechanical conformity to biological surfaces. The thin and flexible architecture of the sensor will facilitate rapid temperature equilibration, allowing for precise and dynamic skin temperature measurement. Furthermore, the integration of Flex-IC components in elastomeric substrates opens up possibilities for monitoring a wide range of physical and physiological parameters, paving the way for next-generation wearable health monitoring devices.

II. System Architecture

The Flex-IC technology offers a reduced subset of components compared to traditional CMOS technologies. Namely,

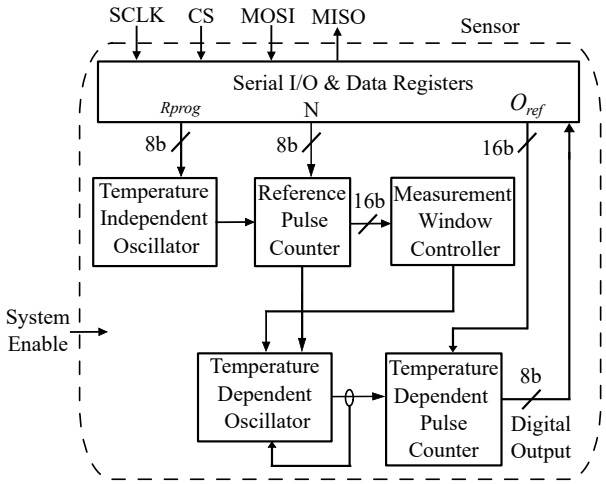

Fig. 1. The flexible temperature sensor block diagram showing the oscillators implementing the TDC architecture.

thin film NMOS transistors, resistors, and capacitors. This requires creative circuit design approaches to implement the desired functionality in the technology. The presented sensor architecture implements a temperature estimation function based on the ratio of two periods, which serves as the core temperature sensing mechanism. Similar approaches have been successfully implemented in previous work [12], [13], [14]. The system functions as a TDC by counting the pulses of a temperature-dependent oscillator within a fixed observation window, which is defined by a temperature-independent reference period, through the structure depicted in Figure 1.

In this figure, the temperature-dependent ring oscillator, composed of three NMOS inverter stages with resistive loads, generates a frequency that varies directly with temperature. The relationship is manifested by Pragmatic Semiconductor's native resistor that exhibits a positive temperature coefficient. The temperature-independent reference oscillator is composed of seven fully differential amplifiers in a ring formation. Temperature independence is established by ensuring that the RC time constant does not vary with temperature, where R is the amplifier's output impedance and C is the parasitic capacitance between stages. To achieve this, the differential amplifier features an output stage based on the tunable negative impedance topology [15]. Further design details of the temperature sensor is provided in Section III.

In the counter-based TDC approach presented, the temperature-dependent pulse counter is disabled when the reference pulse counter reaches a digitally programmed count value, referred here as precision factor N. The time between initialization and disable is defined as the measurement window. The final digital output Y approximates the temperature through the product of the temperature-dependent oscillator frequency f_r and the reference oscillator period P_w, scaled by N and shifted by the output reference O_{ref}, as described in Equation 1, effectively translating the temperature information into an equivalent digital format.

$$Y = NP_w f_r - O_{\text{ref}}, \tag{1}$$

III. Sensor Design and Implementation

A. Temperature-independent Reference Oscillator

A temperature-independent oscillator provides a stable time reference for the sensor. The delay cell is composed of a series of fully differential components in a ring, enabling oscillation. The differential amplifier's circuit schematic is shown in Figure 2 and consists of a differential input pair, Q_1 and Q_2, cross-coupled pair, Q_4 and Q_5, and a programmable bias current source.

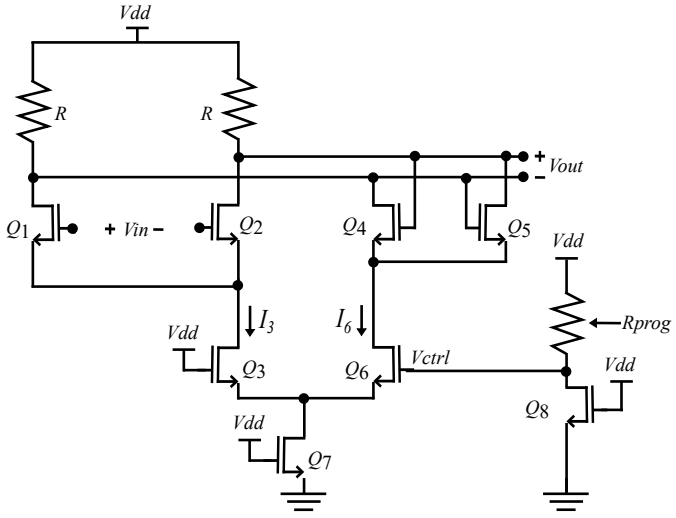

Fig. 2. The schematic of a single delay element used in the temperature-independent reference oscillator.

The period of the reference oscillator is established by the RC time constant of the system. Resistors employed by Flex-IC technology exhibit a positive temperature coefficient, which is nulled using the negative coefficient exhibited by the cross-coupled transistor pair's small signal resistance $r_{cc} = -\frac{2}{g_m}$, where g_m is the transconductance of Q_4 and Q_5 and it is adjustable via bias current I_6. This enables the output stage to compensate for the inherent temperature dependence of the resistors, ensuring the effective resistance is constant and the complete circuit has stable delay performance across varying thermal conditions, as discussed later in Section III-B.

The goal of the circuit design is for both R and r_{cc} to scale by the same factor in opposite directions within a given temperature change, causing the resistance of their parallel combination to be constant. This is achieved through temperature-dependent current steering. To realize this impedance balance mechanism, let's define α as the resistor's temperature coefficient, set by the technology, and β as temperature coefficient of r_{cc}. Output impedance at a single output node of the differential amplifier is the parallel combination of R and -$\frac{1}{g_m}$, shown by Equation 2, which gives output impedance as a function of temperature.

$$R_{out}(T) = \frac{(R(1+\alpha T)\frac{1}{g_m}(1+\beta T)}{\frac{1}{g_m}(1+\beta T) - R(1+\alpha T)} \tag{2}$$

By definition, if the circuit's output impedance is independent of temperature, it should be constant within

the desired temperature operation range, $[0, T_1]$. With this condition, β is defined by Equation 3, approximated due to small α.

$$\beta = \frac{\alpha \frac{1}{g_m}}{R + \alpha T_1 (R - \frac{1}{g_m})} \approx \frac{\alpha}{R g_m} \tag{3}$$

In Figure 2, a temperature-dependent current I_6 is used to bias r_{cc} and achieve the desired temperature coefficient β. The temperature dependence of I_6 is dictated by V_{ctrl}. As R varies with temperature, R_{prog} varies proportionally, causing V_{ctrl} to vary inversely with R_{prog}. This inverse relationship allows V_{ctrl} to dynamically adjust r_{cc}. As I_6 increases, r_{cc} becomes less negative, thereby increasing its contribution to overall output impedance. This counteracts the temperature-induced variation in R, as expressed in Equation 2. Since on-chip resistors exhibit the strongest temperature variation, β is primarily determined by the variation of R_{prog}. This mechanism is leveraged to combat the temperature dependence native to on-chip resistors. A key design feature of this circuit is the differential variation of I_3 and I_6 with their sum held constant. This ensures that the total current steered between the differential load resistors R remains constant across the tuning range, maintaining a constant output swing.

B. Calibration

To mitigate process variations inherent to the fabrication, calibration mechanisms are required. There are three calibration techniques exercised: Linearization Control R_{prog}, Precision Factor N, and output reference O_{ref}. Once all three calibration techniques are applied, the digital output becomes linear with programmable slope and offset with respect to temperature across all process variation extremes.

Linearization control is achieved by setting the 8-bit programmable resistance R_{prog} shown in Figure 2. V_{ctrl} varies inversely with R_{prog}, which in turn changes the bias current to the differential amplifier, adjusting the $\frac{1}{g_m}$ term in Equation 2. As a result, the temperature independence of the circuit is calibrated regardless of the specific process corner at which a chip sample is fabricated.

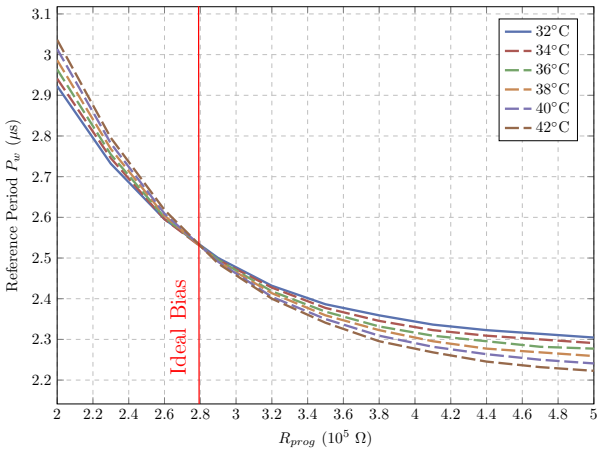

Fig. 3. The R_{prog} resistance adjusts the duration of the measurement window. The time duration becomes temperature-independent when calibrated to the intersection of the family of temperature curves.

Figure 3 displays the reference period in seconds as a function of R_{prog}. Multiple curves are shown, corresponding to various body temperatures, which define the input range for a potential application. The intersection of these curves represents the optimal bias point because it is here that the reference period length is constant across temperatures.

The precision factor enables a digitally programmable, user adjustable measurement window duration N. This sets the slope of the plots in Figure 4. This form of calibration provides resilience to process variations by allowing for compensation of the delay mismatch between chip samples. Additionally, this enables the option of finer control defined by the application's requirements. The output reference O_{ref} sets the initial value of the temperature-dependent pulse counter. Setting this to a negative value enables the system to be calibrated for any offset.

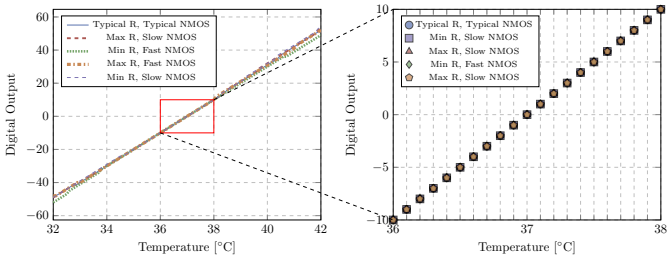

Fig. 4. Circuit simulations show a linear sensor response. Calibration corrects for nonlinearities associated with process corners across the targeted temperature range used for biological sensing.

Simulation results, shown in Figure 4, demonstrate that the sensor achieves a precision of $0.1\,^{\circ}\mathrm{C}$ and an accuracy of $0.2\,^{\circ}\mathrm{C}$ over a $10\,^{\circ}\mathrm{C}$ range. There is a trade-off between accuracy and precision, and the sensor can be calibrated to optimize one over the other based on the specific requirements of the application. Accuracy, defined as the difference between observed and expected output, can be adjusted to center the zero-error region around any temperature. At $37\,^{\circ}\mathrm{C}$, the sensor exhibits a zero-error range of $6.8\,^{\circ}\mathrm{C}$, ensuring reliable performance within the calibrated region despite process variations.

C. Layout and I/O Interface

The chip layout displayed in Figure 5, measuring $3.0\,\mathrm{mm} \times 3.0\,\mathrm{mm}$, integrates both the temperature-dependent and temperature-independent oscillators along with their associated logic. The design includes I/O pads for control, calibration, and testability. A serial interface is implemented to minimize the number of pads, with data lines handling both calibration and readout

IV. Simulation Results

Extracted simulation results of the chip demonstrate that it achieves a measurement time of $3\,\mathrm{ms}$ with a precision of $0.1\,^{\circ}\mathrm{C}$ and accuracy of $0.2\,^{\circ}\mathrm{C}$ over a $10\,^{\circ}\mathrm{C}$ range. During active operation, the system consumes $2.5\,\mathrm{mW}$ of power, necessitated by the resistive loads. However, the power consumption will decrease proportionally with the duty cycle, as the chip only requires power while sensing. The frequency of

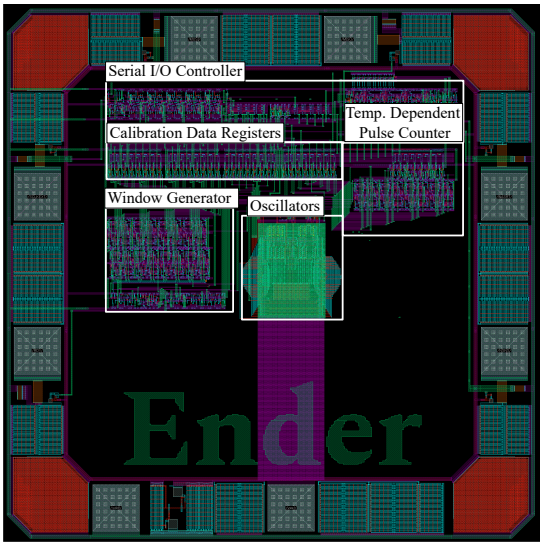

Fig. 5. Temperature Sensor Chip Layout. The dimensions are $3\,\mathrm{mm} \times 3\,\mathrm{mm}$.

the temperature-dependent oscillator drifts between $550\,\mathrm{kHz}$ and $590\,\mathrm{kHz}$ over the temperature range of $32\,^{\circ}\mathrm{C}$ to $42\,^{\circ}\mathrm{C}$, while the reference oscillator maintains a stable frequency of $570\,\mathrm{kHz}$, enabling efficient and accurate temperature measurements in biological environments.

A. Noise Analysis

Electronic noise introduces measurement error through jitter in the temperature-dependent oscillator and the temperature-independent reference. The jitter in both circuits is characterized by their standard deviations σ_r (temperature-dependent oscillator) and σ_w (temperature-independent reference). Both sources of jitter are assumed to be Gaussian distributed with a mean of zero.

The total system jitter, σ_{total}, can be expressed as the root-sum-square of the individual jitter components. Jitter contributions from the temperature-dependent oscillator and temperature-independent reference are uncorrelated. Therefore, a closed form expression for the total jitter variance is defined in Equation 4.

$$\sigma^2_{\text{total}} = N\sigma^2_w + (Y - O_{ref})\sigma^2_r \tag{4}$$

In addition to the jitter contributions, the relative time difference between the end of the measurement window and the next oscillator edge serves as the threshold that jitter must exceed in order to achieve a least significant bit (LSB) toggle. This time difference can be represented as a uniform random variable ΔT with range [-$\frac{1}{2f_r}$, $\frac{1}{2f_r}$].

The probability of an LSB toggle error caused by total jitter can be determined by taking twice the average of the survival function of a standard Gaussian distribution over the right half of the uniform distribution of ΔT, leveraging the system's symmetry. This probability is expressed in Equation 5 where $\Phi(x)$ is the standard Gaussian cumulative distribution function, and σ_{total} is the total jitter standard deviation [16].

$$\Pr(\text{Error}) = 2f_r \int_0^{\frac{1}{2f_r}} \left(1 - \Phi\left(\frac{\Delta T}{\sigma_{\text{total}}}\right)\right) d(\Delta T) \tag{5}$$

Through noise simulations, σ_w and σ_r are measured to be $284\,\mathrm{ps}$ and $312\,\mathrm{ps}$ with f_r of $573\,\mathrm{kHz}$. For a typical sample, $0.1\,^{\circ}\mathrm{C}$ precision is achieved with an N and Y of about $1.7\,\mathrm{k}$ and $1.8\,\mathrm{k}$, respectively. Therefore, the probability of a jitter induced LSB toggle is $0.81\,\%$ per sample.

V. Conclusion and Future Work

The design of a completely flexible temperature sensor for wearable applications is presented. The sensor is implemented using the recently available Flex-IC fabrication technology from Pragmatic Semiconductor, which offers a limited set of non-CMOS thin film components. To address the design challenges due to this limitation, a counter-based TDC approach has been considered by the authors. To that end, the pulses provided by a temperature-dependent ring oscillator are gated and counted by a temperature-independent delay cell producing a linear digital representation of the temperature.

The presented design approach for the delay cell employed in gating the counts relies on the temperature coefficient cancellation of resistive components by a cross-coupled pair. Moreover, the design incorporates a calibration mechanism in order to handle variations due to process corners across a $32\,^{\circ}\mathrm{C}$ - $42\,^{\circ}\mathrm{C}$ temperature range with minimal time jitter interference. Compared to existing rigid and hybrid systems, the Flex-IC technology opens up opportunities for advancing conformal electronics and addressing current challenges in robustness, functionality, and form factor, particularly for applications requiring continuous monitoring on dynamic body surfaces.

Future work involves encapsulation of the fabricated Flex-IC prototype in an ultralow modulus silicone elastomer, where various strategies such as spin processing and injection molding will be considered. These methods will allow for precise control over the encapsulation thickness. For testing and characterization, interconnects with a minimum width and pitch of $100\,\mu\mathrm{m}$ will be created from patterned serpentine architectures using copper film and room-temperature liquid metal electrical wiring based on the previous work by the authors [6], [17], [18]. These methods will provide a highly robust electrical connectivity between the Flex-IC and external measurement instruments and power supplies.

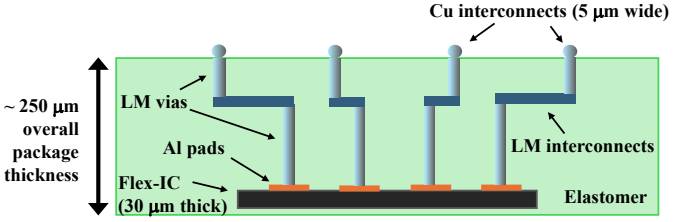

Fig. 6. Flex-IC Encapsulation Methodology.

The cross-section of the aforementioned encapsulation methodology is shown in Figure 6, where an overall flexible package thickness of $250\,\mu\mathrm{m}$ is planned based on the similar dimensions employed in previous work.

REFERENCES

[1] Pragmatic Semiconductor, "Flexible Integrated Circuits and Systems," [Online] https://www.pragmaticsemi.com.

[2] M. Kaltenbrunner, T. Sekitani, J. Reeder, T. Yokota, K. Kuribara, T. Tokuhara, M. Drack, R. Schwödiauer, I. Graz, S. Bauer-Gogonea, S. Bauer, and T. Someya, "An ultra-lightweight design for imperceptible plastic electronics," *Nature*, vol. 499, no. 7459, p. 458–463, Jul. 2013. [Online]. Available: http://dx.doi.org/10.1038/nature12314

[3] T. Sekitani, U. Zschieschang, H. Klauk, and T. Someya, "Flexible organic transistors and circuits with extreme bending stability," *Nature Materials*, vol. 9, no. 12, p. 1015–1022, Nov. 2010. [Online]. Available: http://dx.doi.org/10.1038/nmat2896

[4] Luo, "Technology roadmap for flexible sensors," *ACS Nano*, vol. 17, no. 6, p. 5211–5295, Mar. 2023. [Online]. Available: http://dx.doi.org/10.1021/acsnano.2c12606

[5] Z. Huang, Y. Hao, Y. Li, H. Hu, C. Wang, A. Nomoto, T. Pan, Y. Gu, Y. Chen, T. Zhang, W. Li, Y. Lei, N. Kim, C. Wang, L. Zhang, J. W. Ward, A. Maralani, X. Li, M. F. Durstock, A. Pisano, Y. Lin, and S. Xu, "Three-dimensional integrated stretchable electronics," *Nature Electronics*, vol. 1, no. 8, p. 473–480, Aug. 2018. [Online]. Available: http://dx.doi.org/10.1038/s41928-018-0116-y

[6] E. Markvicka, G. Wang, Y.-C. Lee, G. Laput, C. Majidi, and L. Yao, "Electrodermis: Fully untethered, stretchable, and highly-customizable electronic bandages," in *Proceedings of the 2019 CHI Conference on Human Factors in Computing Systems*, ser. CHI '19. ACM, May 2019, p. 1–10. [Online]. Available: http://dx.doi.org/10.1145/3290605.3300862

[7] J. W. Lee, R. Xu, S. Lee, K.-I. Jang, Y. Yang, A. Banks, K. J. Yu, J. Kim, S. Xu, S. Ma, S. W. Jang, P. Won, Y. Li, B. H. Kim, J. Y. Choe, S. Huh, Y. H. Kwon, Y. Huang, U. Paik, and J. A. Rogers, "Soft, thin skin-mounted power management systems and their use in wireless thermography," *Proceedings of the National Academy of Sciences*, vol. 113, no. 22, p. 6131–6136, May 2016. [Online]. Available: http://dx.doi.org/10.1073/pnas.1605720113

[8] Z. Dou, D. Richmond, M. Schadt, M. Alhendi, R. Al-Haidari, R. Tudela, and M. Poliks, "Evaluation of electromechanical performance of a flexible hybrid electronics temperature monitor," in *2023 IEEE 73rd Electronic Components and Technology Conference (ECTC)*. IEEE, May 2023, p. 2213–2217. [Online]. Available: http://dx.doi.org/10.1109/ECTC51909.2023.00383

[9] W.-P. Shih, L.-C. Tsao, C.-W. Lee, M.-Y. Cheng, C. Chang, Y.-J. Yang, and K.-C. Fan, "Flexible temperature sensor array based on a graphite-polydimethylsiloxane composite," *Sensors*, vol. 10, no. 4, p. 3597–3610, Apr. 2010. [Online]. Available: http://dx.doi.org/10.3390/s100403597

[10] M. D. Husain, R. Kennon, and T. Dias, "Design and fabrication of temperature sensing fabric," *Journal of Industrial Textiles*, vol. 44, no. 3, p. 398–417, Jul. 2013. [Online]. Available: http://dx.doi.org/10.1177/1528083713495249

[11] S. Khan, L. Lorenzelli, and R. S. Dahiya, "Technologies for printing sensors and electronics over large flexible substrates: A review," *IEEE Sensors Journal*, vol. 15, no. 6, p. 3164–3185, Jun. 2015. [Online]. Available: http://dx.doi.org/10.1109/JSEN.2014.2375203

[12] Z. Tang, Y. Fang, Z. Shi, X.-P. Yu, N. N. Tan, and W. Pan, "A 1770-μ m2 leakage-based digital temperature sensor with supply sensitivity suppression in 55-nm cmos," *IEEE Journal of Solid-State Circuits*, vol. 55, no. 3, p. 781–793, Mar. 2020. [Online]. Available: http://dx.doi.org/10.1109/JSSC.2019.2952855

[13] Y.-S. Lin, D. Sylvester, and D. Blaauw, "An ultra low power 1v, 220nw temperature sensor for passive wireless applications," in *2008 IEEE Custom Integrated Circuits Conference*, vol. 40. IEEE, Sep. 2008, p. 507–510. [Online]. Available: http://dx.doi.org/10.1109/CICC.2008.4672133

[14] S. Jeong, Z. Foo, Y. Lee, J.-Y. Sim, D. Blaauw, and D. Sylvester, "A fully-integrated 71 nw cmos temperature sensor for low power wireless sensor nodes," *IEEE Journal of Solid-State Circuits*, vol. 49, no. 8, p. 1682–1693, Aug. 2014. [Online]. Available: http://dx.doi.org/10.1109/JSSC.2014.2325574

[15] J. Linvill, "Transistor negative-impedance converters," *Proceedings of the IRE*, vol. 41, no. 6, p. 725–729, Jun. 1953. [Online]. Available: http://dx.doi.org/10.1109/JRPROC.1953.274251

[16] A. Hajimiri, S. Limotyrakis, and T. Lee, "Jitter and phase noise in ring oscillators," *IEEE Journal of Solid-State Circuits*, vol. 34, no. 6, p. 790–804, Jun. 1999. [Online]. Available: http://dx.doi.org/10.1109/4.766813

[17] C. Pan, K. Kumar, J. Li, E. J. Markvicka, P. R. Herman, and C. Majidi, "Visually imperceptible liquid-metal circuits for transparent, stretchable electronics with direct laser writing," *Advanced Materials*, vol. 30, no. 12, Feb. 2018. [Online]. Available: http://dx.doi.org/10.1002/adma.201706937

[18] M. D. Bartlett, E. J. Markvicka, and C. Majidi, "Rapid fabrication of soft, multilayered electronics for wearable biomonitoring," *Advanced Functional Materials*, vol. 26, no. 46, p. 8496–8504, Sep. 2016. [Online]. Available: http://dx.doi.org/10.1002/adfm.201602733